

Precise control of phase transformation process in lead zirconate titanate thin films by focused line-beam scanning

Jang-Sik Lee, Jung-Kun Lee, and Seung-Ki Joo

Citation: [Applied Physics Letters](#) **90**, 132908 (2007); doi: 10.1063/1.2719636

View online: <http://dx.doi.org/10.1063/1.2719636>

View Table of Contents: <http://scitation.aip.org/content/aip/journal/apl/90/13?ver=pdfcov>

Published by the [AIP Publishing](#)

Articles you may be interested in

[Phase transformation and crystallization kinetics of a-Ge/Cu bilayer for blue-ray recording under thermal annealing and pulsed laser irradiation](#)

J. Appl. Phys. **111**, 043503 (2012); 10.1063/1.3684966

[Deposition of sol-gel derived lead lanthanum zirconate titanate thin films on copper substrates](#)

Appl. Phys. Lett. **92**, 252905 (2008); 10.1063/1.2945887

[Phase transformation and freestanding nanoparticles formation in lead zirconate titanate derived by sol-gel](#)

Appl. Phys. Lett. **91**, 063115 (2007); 10.1063/1.2768626

[Structure of electroless deposited Co_{0.9}W_{0.02}P_{0.08} thin films and their evolution with thermal annealing](#)

J. Appl. Phys. **94**, 3810 (2003); 10.1063/1.1602572

[Self-limiting behavior of the grain growth in lead zirconate titanate thin films](#)

J. Appl. Phys. **92**, 2658 (2002); 10.1063/1.1496147

A banner for the 2014 Special Topics section of Applied Physics Letters. The banner is orange and features five circular icons representing different material categories: Perovskites, 2D Materials, Mesoporous Materials, Biomaterials/Bioelectronics, and Metal-Organic Framework Materials. The text '2014 Special Topics' is prominently displayed in the center. At the bottom left is the 'AIP | APL Materials' logo, and at the bottom right is a red ribbon with the text 'Submit Today!'.

Precise control of phase transformation process in lead zirconate titanate thin films by focused line-beam scanning

Jang-Sik Lee^{a),b)}

School of Advanced Materials Engineering, Kookmin University, Seoul 136-702, Korea

Jung-Kun Lee

Los Alamos National Laboratory, Los Alamos, New Mexico 87545

Seung-Ki Joo^{a),c)}

School of Materials Science and Engineering, College of Engineering, Seoul National University, Seoul 151-742, Korea

(Received 13 December 2006; accepted 3 March 2007; published online 30 March 2007)

Phase transformation and grain growth processes of lead zirconate titanate (PZT) thin films have been precisely controlled by using focused line-beam scanning. The authors promoted the lateral crystallization of PZT grains by controlling a nucleation process and increasing the size of single grains to be as large as 40 μm in length. Focused line-beam scanning allows for the selective growth and crystallization of large PZT grains on predetermined nucleation sites. The high growth rate of the selected PZT grains was attributed to successive suppression of undesirable nucleation except at predetermined positions when pretreated PZT films were exposed to the focused line beam. © 2007 American Institute of Physics. [DOI: 10.1063/1.2719636]

We previously reported the selectively nucleated lateral crystallization (SNLC) of $\text{Pb}(\text{Zr}, \text{Ti})\text{O}_3$ (PZT) thin films and their electrical characteristics.¹⁻³ By SNLC method, we could control the nucleation site, thereby the grain location in PZT thin films. SNLC was based on the selective nucleation and grain growth between the template layer and the perovskite seed. However, the selective growth of the large grains by using the conventional annealing method has a limitation because the annealing temperature should be low enough to prevent undesirable nucleation at unseeded region, resulting in very low growth rate. Also, even though the annealing temperature is lower than the normal growth temperature of the PZT grains, there is still undesirable nucleation at sites where the pretreated seeds are not present. Therefore, an annealing method, i.e., scanning rapid thermal annealing (RTA), is used in this study to prevent the undesirable nucleation by reducing the processing time. Here, we report the mechanism for SNLC of PZT films and discuss the effect of scan-lamp power and scan speed on their crystallization and microstructure.

$\text{PbZr}_{0.65}\text{Ti}_{0.35}\text{O}_3$ thin films were formed on Pt/SiO₂/Si substrates by rf magnetron sputtering at 350 °C using multimetall targets of Pb, Zr, and Ti. A base pressure before sputtering was below 1×10^{-5} Torr. The detailed deposition conditions can be found elsewhere.¹⁻³ A PZT thin film (100 nm) as the seeding layer was deposited on Pt/SiO₂/Si substrate and transformed into the perovskite phase by RTA. Seeding islands (area: $10 \times 10 \mu\text{m}^2$, spaces: 40 and 60 μm) were patterned by a conventional lithographic and etching method. A PZT thin film (200 nm) was then deposited on the substrate having PZT seeding islands. The growth behavior of the films was investigated using a Nomarski microscope with differential interference contrast. The microstructure and

crystal phases of the PZT films were determined using transmission electron microscopy (TEM) and x-ray diffractometer, respectively.

SNLC annealing was carried out by scanning RTA with tungsten-halogen lamps. A line-shaped light, which was focused with an elliptical reflector, was scanned over the specimen that had been preheated by bottom lamps. The temperature was monitored by a computer-based temperature measurement system connected with a thermocouple located at the side of the specimen. Figure 1 shows the three-dimensional illustration of the scanning-RTA apparatus with the schematic temperature profile and its direction. The local part of the sample was heated at high temperature and the

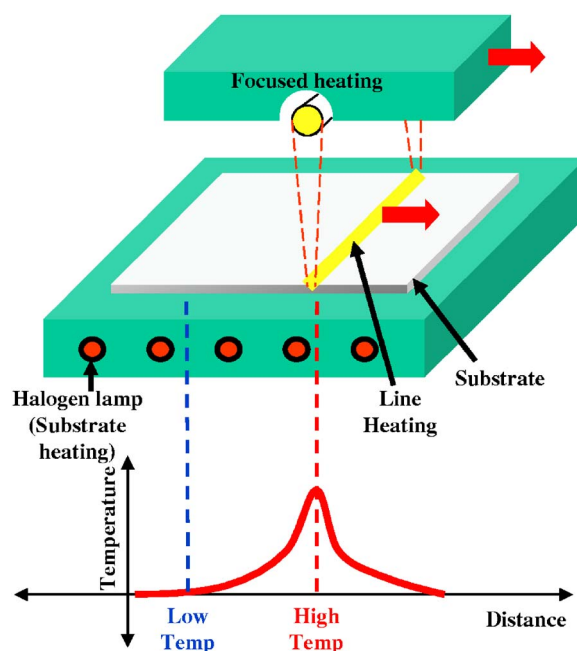


FIG. 1. (Color online) Three-dimensional illustration of the scanning-RTA apparatus with the schematic temperature profile and scanning direction.

^{a)} Authors to whom correspondence should be addressed.

^{b)} Electronic mail: jangsik@kookmin.ac.kr

^{c)} Electronic mail: skjoo@plaza.snu.ac.kr

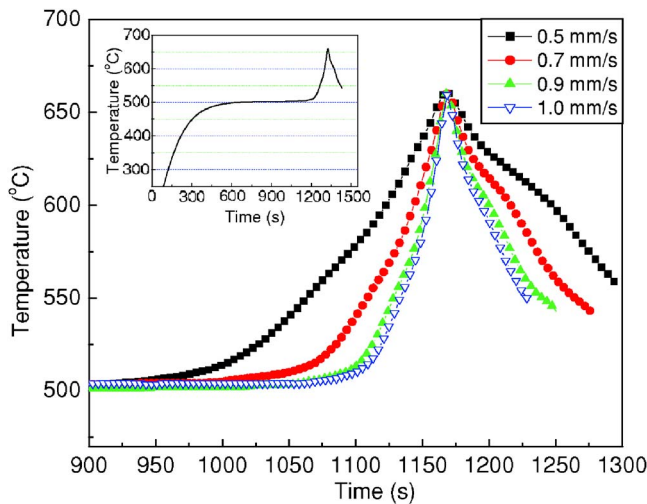


FIG. 2. (Color online) Temperature profiles according to the scan speed from 0.5 to 1 mm/s. The inset figure shows the whole temperature profile for scan speed of 0.7 mm/s.

other part was maintained at low temperature. It is observed that the temperature profiles during scanning-RTA process become narrower as the scan speed is increased at constant upper lamp power. It is also found that peak temperature highly depends on lamp power at constant scan speed.⁴ Therefore, it is possible to adjust the annealing condition to minimize undesirable nucleation and, at the same time, expose the sample to a high temperature for a short period of time.

When the upper lamp scanned the substrate which was preheated at around 500 °C, the substrate experienced steep heating and cooling. Figure 2 shows the measured temperature-time profiles of scanning-RTA processes for scan speed from 0.5 to 1 mm/s. As shown in the temperature profiles, the increase in the scan speed caused a drastic change in the temperature at a fiducial point of peak temperature. The inset figure shows the whole temperature profile of the substrate when the scan speed was 0.7 mm/s. It is clear that, in each scanning, the substrate is exposed to the highest temperature for less than a few seconds. The peak temperature was controlled to be 660 °C exactly for several different scan speed conditions by adjusting the lamp power.

For the preliminary study, we used the PZT thin films with partially grown grains (average grain size of 7 μm) formed after annealing at 680 °C for 1 min. The results are shown in Fig. 3. The inner circles in Fig. 3 present partially crystallized grains, which act as seeds for further grain growth during the scanning-RTA process. The PZT films were exposed to the temperature profiles in Fig. 2. The pre-heating temperature of the sample was around 500 °C, and the scan speed was varied from 0.5 to 1 mm/s with the same peak temperature of 660 °C. The grain growth occurred only at the pre-nucleated regions. Figures 3(a)–3(d) clearly show that the perovskite phase in the PZT films started to grow from the preexistent seeds during the line scanning. As the scan speed decreased from 1 to 0.5 mm/s, the SNLC length increased from about 4 to 20 μm. It was noticed that there was no undesirable nucleation other than the pre-nucleated regions at the peak temperature of as high as 660 °C. The annealing temperature could not be increased over 600 °C in the case of conventional furnace annealing because undesirable nucleation became significant.^{1,2} It was also found that

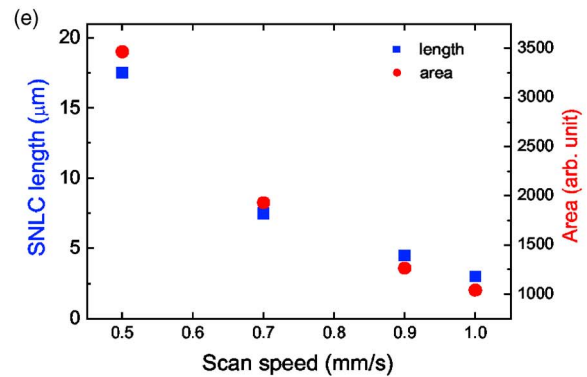
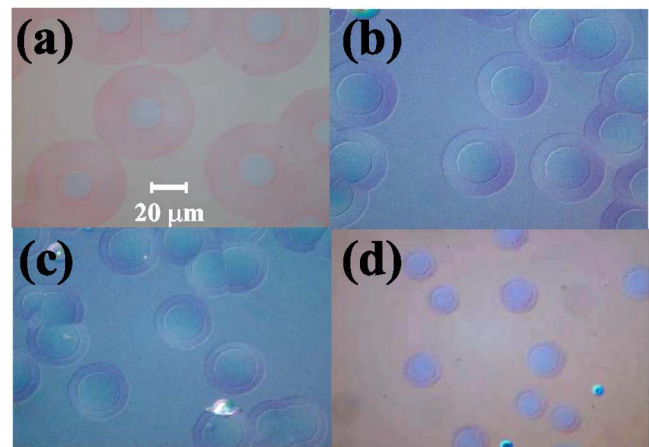


FIG. 3. (Color online) SNLC of PZT thin films using partially grown grains as seeds with scan speeds of (a) 0.5 mm/s, (b) 0.7 mm/s, (c) 0.9 mm/s, and (d) 1.0 mm/s. (e) Dependence of SNLC length and the integral area of temperature profiles above 600 °C on the scan speed.

the growth rate of the line-beam scanning was very fast as compared with that of the conventional furnace annealing ($\sim\mu\text{m/s}$ vs $\sim\mu\text{m/h}$).² The activation energy of the nucleation is generally higher than that of the grain growth.⁵ SNLC process exploits this difference in the activation energy between the nucleation and grain growth. It is easily noticed that the higher the energy is, the faster the grain growth is. However, the probability for the nucleation of the PZT grains in the unseeded region is also proportional to the thermal energy. Therefore, the increase in the annealing temperature results in a conflict between the growth rate and the selectivity in SNLC process. If it is possible to apply high energy for a very short period at only desired position with other regions being at low temperature, undesirable nucleation outside the predetermined sites can be minimized. Figure 3(e) shows the SNLC length measured from Figs. 3(a)–3(d) and the integral area of the region above 600 °C in the temperature profiles (Fig. 2) as a function of the scan speed. Both of the SNLC length and the area of the scanned region above 600 °C are inversely proportional to the scan speed. The integral area of temperature profiles is directly related to the heat transferred to the PZT films, which is believed to drive the grain growth.

From the preliminary study using partially grain-grown PZT thin films, the scanning-RTA process was found to be very feasible and effective method to realize SNLC. Thus, the scanning RTA for SNLC was done for the PZT films with etched seeds to align the position of the largely grown grains. The scan speed was 0.5 mm/s whose temperature profile was shown in Fig. 2. Figure 4(a) shows the lateral crystalli-

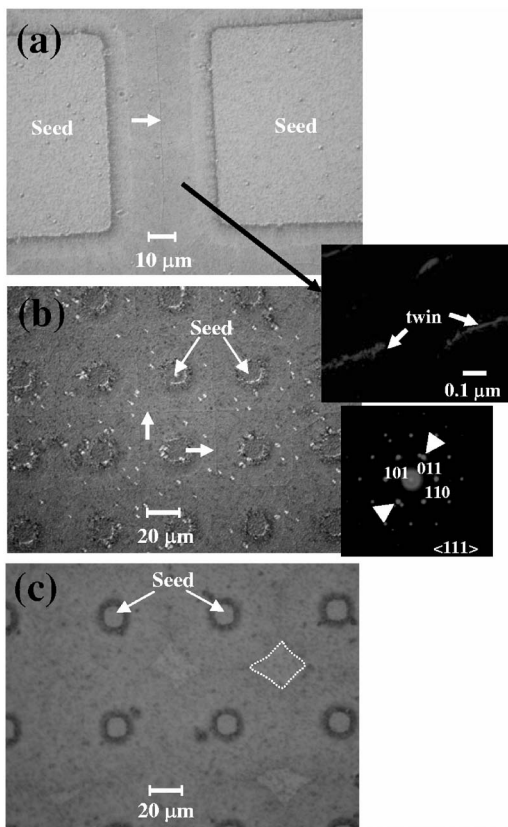


FIG. 4. SNLC of PZT thin films using PZT seeding method. (a) Completion of SNLC with line boundary. Arrays of single-grained PZT thin films for the distance between adjacent seeds of (b) $40\ \mu\text{m}$ and (c) $60\ \mu\text{m}$. The inset shows the TEM images of the laterally crystallized region and its $\langle 111 \rangle$ SAED pattern.

zation began from the edge of the PZT seeds and ended after making a line grain boundary between seeds (see the arrow). The grown length was about $20\ \mu\text{m}$. The SNLC with small seeds of $10 \times 10\ \mu\text{m}^2$ is shown in Fig. 4(b). The square pattern of the single-grained PZT thin films can be clearly seen. Figure 4(c) shows the SNLC of PZT films when the distance between the seeds was as large as $60\ \mu\text{m}$. The laterally grown length was $25\ \mu\text{m}$ keeping the shape of the seed in view. The crystallization was not completed and the noncrystallized region was shown in lozenge shape. We have measured the electrical properties of PZT thin films selectively crystallized by the scanning-RTA process using the sample shown in Fig. 4(b). The Pt top electrode location was precisely controlled to be aligned inside the grains. The ferroelectric and conduction properties were almost the same as those we previously reported.³ Thus, by utilizing scanning-RTA process, it is possible to obtain high-quality single-

grained PZT thin films with almost complete selectivity in grain growth.

Transmission electron micrograph of the laterally crystallized region in PZT thin films is also presented in the insets of Fig. 4. The micrograph was taken using the sample of Fig. 4(a). It shows almost clean matrix except the small lamellae-type defects. To verify the kinds of line defects, selected area electron diffraction (SAED) analysis was carried out. The corresponding electron diffraction pattern in the other inset of Fig. 4 represents a perovskite single-crystalline pattern viewing along the $\langle 111 \rangle$ direction. Macroscopic rhombohedral symmetry can be preserved by averaging in over many small ordered regions with $\langle 110 \rangle$ structural modulations.⁶ Twin spots were observed along the plane of $\{101\}$, indicating that the lamellae-type defects in the laterally crystallized region were twin boundaries. These twins might form during SNLC to reduce the strain energy of the large grains.⁷⁻¹⁰

PZT thin films with large and position-controlled grains could be obtained by combining the focused line-beam scanning and the seeding method. We show that the grain boundary location in PZT films could be determined by controlling the seed location and the thermal annealing conditions. The thermal profiles could be controlled by changing the scan speed and the lamp power, which directly affected the SNLC process. It was found that scanning RTA was very feasible and to be an effective method for SNLC in reducing the processing time, preventing undesirable nucleation other than the predetermined positions, and in turn increasing the growth rate.

Work performed at the Kookmin University was supported from the Center for Materials and Processes of Self-Assembly (R11-2005-048-00000-0) by the ERC program of MOST/KOSEF. This work was also supported in part by the New Faculty Research Program 2006 of Kookmin University in Korea.

¹J.-S. Lee and S.-K. Joo, Jpn. J. Appl. Phys., Part 1 **39**, 6343 (2000).

²J.-S. Lee and S.-K. Joo, J. Appl. Phys. **92**, 2658 (2002).

³J.-S. Lee and S.-K. Joo, Appl. Phys. Lett. **81**, 2602 (2002).

⁴J.-S. Lee and S.-K. Joo, Mater. Res. Soc. Symp. Proc. **688**, C1.3 (2002).

⁵C. K. Kwok and S. B. Desu, J. Mater. Res. **9**, 1728 (1994).

⁶D. Viehland, Phys. Rev. B **52**, 778 (1995).

⁷P.-H. Chang, G. Berman, and C. C. Shen, J. Appl. Phys. **63**, 1473 (1988).

⁸J. D. Verhoeven, E. D. Gibson, L. S. Chumbley, R. W. McCallum, and H. H. Baker, J. Appl. Phys. **64**, 761 (1988).

⁹A. Nakamura, F. Emoto, E. Fujii, A. Yamamoto, Y. Uemoto, K. Senda, and G. Kano, J. Appl. Phys. **66**, 4248 (1989).

¹⁰L. D. Madsen, E. M. Griswold, and L. Weaver, J. Mater. Res. **12**, 2612 (1997).